Conversion of highly polymerized lignin into monophenolic products via pyrolysis: A comparative study of acidic and alkaline depolymerization pretreatments using deep eutectic solvents

Yue, Xin; Lin, Jinxin; Suopajärvi, Terhi; Mankinen, Otto; Mikkelson, Atte; Liu, Rui; Huttunen, Harri; Chen, Liheng; Xu, Chunlin; Telkki, Ville-Veikko; Sun, Shirong; Liimatainen, Henrikki

Published in:
Chemical Engineering Journal

DOI:
10.1016/j.cej.2023.147368

Published: 15/12/2023

Document Version
Final published version

Document License
CC BY

Chemical Engineering Journal 478 (2023) 147368

Contents lists available at ScienceDirect

Chemical Engineering Journal

journal homepage: www.elsevier.com/locate/cej

Conversion of highly polymerized lignin into monophenolic products via pyrolysis: A comparative study of acidic and alkaline depolymerization pretreatments using deep eutectic solvents

Xin Yue [a,1], Jinxin Lin [b,1], Terhi Suopajärvi [a], Otto Mankinen [c], Atte Mikkelson [d], Rui Liu [e], Harri Huttunen [f], Liheng Chen [b], Chunlin Xu [e], Ville-Veikko Telkki [c], Shirong Sun [b,*], Henrikki Liimatainen [a,*]

[a] Fiber and Particle Engineering Research Unit, University of Oulu, P.O. Box 4300, 90014 Oulu, Finland
[b] School of Chemical Engineering and Light Industry, Guangdong University of Technology, 510006 Guangdong, China
[c] NMR Research Unit, University of Oulu, P.O. Box 4300, 90014 Oulu, Finland
[d] VTT Technical Research Centre of Finland, Vuorimiehentie 3, 02150 Espoo, Finland
[e] Laboratory of Natural Materials Technology, Åbo Akademi University, Henrikinkatu 2, 20500 Turku, Finland
[f] Unit of Measurement Technology MITY, Teknologiapuisto PL 127, 87400 Oulu, Finland

ARTICLE INFO

Keywords:
Deep eutectic solvent
Fast pyrolysis
Hydrolysis lignin
Phenolic compound

ABSTRACT

Converting industrial residual lignin into monophenolic compounds remains a formidable challenge within biorefinery processes, especially when dealing with highly polymerized lignin. This study focuses on the depolymerization of industrial softwood enzyme hydrolysis lignin (SEHL), a by-product of bioethanol production, which possesses a substantial molar mass ($\bar{M}_w$ > 10000 g/mol), The approach involves utilizing acidic or alkaline deep eutectic solvent (DES) for pre-depolymerization, followed by rapid pyrolysis, achieving the selective generation of phenolic monomers. Applying acidic or alkaline DES pretreatments initiates depolymerization by breaking the *β*–aryl ether bonds (*β*–O–4) in lignin, but consequently triggers distinct reaction pathways. It is found that this pre-depolymerization leads to higher yields of phenolic monomers dominated by 4–methylguaiacol during the subsequent pyrolysis, moreover, the yields resulted from acidic DES-lignin were much higher than those from alkaline DES-lignin. We have comprehensively elucidated the lignin depolymerization process during DES pretreatments through computational simulations and experimental investigations. These efforts have provided valuable insights into the mechanisms involved in the structural changes of DES-lignin. Furthermore, we have established a more profound comprehension of how both acidic and alkaline DES pretreatments enhance the performance of lignin pyrolysis. This study emphasizes the importance of thoroughly understanding the intricate interplay between lignin structure and its thermochemical properties. Such insights are crucial for efficiently valorizing highly polymerized lignin to produce valuable phenolic compounds using the rapid pyrolysis technique.

1. Introduction

Renewable and environmentally friendly biofuels derived from lignocelluloses have garnered attention as a means to support the emerging sustainable and circular economies. This heightened interest stems from the limited availability of fossil fuels and the growing concerns regarding the environmental impact of greenhouse gases [1–3]. In particular, bioethanol blends are being hailed as promising next-generation energy sources for transportation owing to their abundance and environmentally clean nature [4,5]. Concurrently, the industrial production of hydrolysis lignin is increasing as a side-stream residue from bioethanol production. Unfortunately, a substantial portion of these lignin residues undergoes incineration in plants, and only a minor fraction (around 1 %–2%) is transformed into bio-based products [6]. Consequently, the effective utilization of residual lignin in value-added products remains a considerable challenge, attracting heightened

* Corresponding authors.
E-mail addresses: shirongsun@gdut.edu.cn (S. Sun), henrikki.liimatainen@oulu.fi (H. Liimatainen).
[1] These authors contributed equally.

https://doi.org/10.1016/j.cej.2023.147368
Received 24 August 2023; Received in revised form 16 October 2023; Accepted 13 November 2023
Available online 18 November 2023

attention within the scientific community.

Lignin constitutes an amorphous and extensively branched aromatic polymer, primarily composed of three distinct C_6–C_3 phenylpropane units with phenolic hydroxyl groups, specifically guaiacyl (G), syringyl (S), and *p*-hydroxyphenyl (H) units. These fundamental subunits are interconnected through various ether and carbon–carbon linkages, such as *β*–O–4, 4–O–5, *α*–O–4, *β*–5, *β*–*β*, *β*–1 [7,8]. Due to these phenylpropane constituents, lignin emerges as the most abundant natural source of aromatic compounds, rendering it a highly valuable biomass feedstock for producing value-added chemicals and renewable biofuels. To date, an array of strategies encompassing combustion, gasification, liquefaction, fermentation, pyrolysis, and carbonization has been devised and implemented for lignin conversion and utilization [9–12]. Fast pyrolysis is a pivotal technology for efficiently depolymerizing lignin with lower capital investment than numerous alternative processes [13]. Generally, lignin pyrolysis occurs within an inert atmosphere (nitrogen or argon) and at elevated temperatures (>400 °C) to rupture the unstable bonds of lignin [14]. Throughout fast pyrolysis, lignin generates diverse low-molecular-weight phenolic compounds. However, the lignin structure considerably influences the distribution and yield of pyrolysis products. Especially, hydrolysis lignin from bioethanol production has a highly crossed-linked and polymerized structure, coupled with an inhomogeneous composition that reduces the efficiency of lignin pyrolysis [15,16].

To overcome these challenges, researchers have dedicated efforts to modifying the structure of hydrolysis lignin before pyrolysis. Methods, such as methylation, acetylation, and oxypropylation have been explored to mitigate the negative influence of oxygen-containing functional groups on pyrolysis [17,18]. However, these techniques often involve harsh reaction conditions and alkalis or acids, which complicate the separation of pyrolysis products, especially concerning pyrolysis bio-oils. Consequently, there is a strong need for efficient and environmentally friendly approaches for recreating hydrolysis lignin. In recent years, deep eutectic solvents (DESs) composed of binary or ternary mixtures of hydrogen bond acceptors (HBA) and hydrogen bond donors (HBD) have garnered extensive attention as sustainable media for enhancing lignin fractionation and valorization. These characteristics can be attributed to their uniqueness, encompassing adjusted chemical attributes, low vapor pressure, low toxicity, and biodegradability [19,20]. DESs have the potential to dissolve hydrolysis lignin and aid its regeneration with a less polymerized structure and lower molar mass. Thus, this in turn aids the conversion of lignin into aromatic phenols. However, the influence of various DES pretreatments on lignin pyrolysis remains inadequately explored.

In this study, we examined the pretreatment of industrial enzymatic hydrolysis lignin from bioethanol production, with a focus on softwood sawdust as the source material. The pretreatment encompassed DES applied through two distinct approaches: acidic treatment involving a combination of lactic acid and choline chloride and alkaline treatment utilizing potassium carbonate and glycerol. The temperature during these reactions was varied, as depicted in Fig. 1. The DES-pretreated lignins were later employed in a fast pyrolysis process to achieve selective monophenolic production. To thoroughly analyze the lignin samples, we used an array of advanced techniques. The chemical composition, functional groups, molar mass, substructures, and inter-unit linkages were assessed using state-of-art methods, including high-performance anion-exchange chromatography (HPAEC), elemental analysis, X-ray photoelectron spectroscopy (XPS), Fourier transform infrared spectroscopy (FT-IR), ^{1}H diffusion ordered nuclear magnetic resonance spectroscopy (DOSY-NMR) as well as 1D ^{13}C- and ^{31}P NMR, and 2D HSQC-NMR. Furthermore, we conducted a thorough examination of the thermal behavior of lignin samples using advanced techniques such as thermogravimetric analysis, pyrolysis and gas chromatography-mass spectrometry (Py–GC/MS) and electron paramagnetic resonance (EPR) spectroscopy. These analyses allowed us to gain valuable insights into the pyrolysis process and the resulting distribution of pyrolyzed compounds. Additionally, we delved into the mechanistic aspects and established the relationship between the distribution of pyrolyzate and the structural modifications induced by DES treatment of hydrolysis lignin. Overall, our study provides a comprehensive elucidation of the impact of lignin heterogeneity on its pyrolysis performance, shedding light on essential factors influencing the overall process.

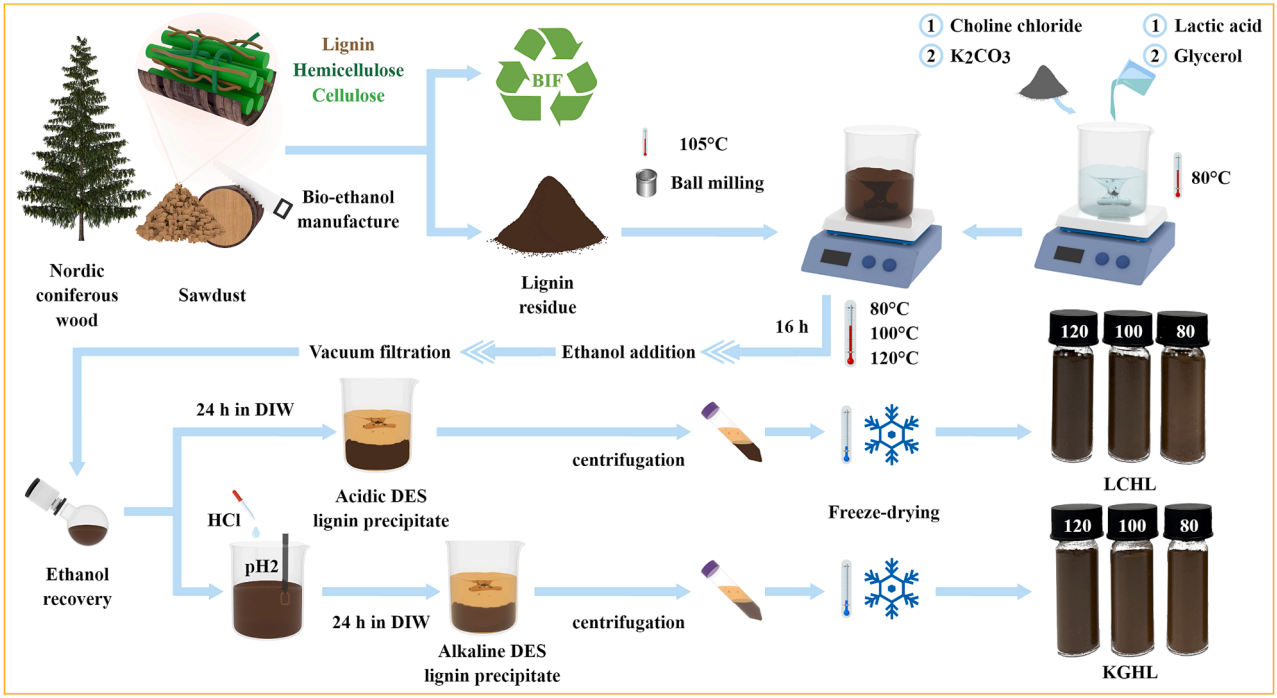

Fig. 1. (a) Pretreatment of the industrial softwood enzyme hydrolysis lignin with DESs. Acronyms used: BIF for biofuel, KGHL for alkaline DES-pretreated lignin, and LCHL for acidic DES-pretreated lignin. (①: acidic DES dissolving system, ②: alkaline DES dissolving system).

2. Material and methods

2.1. Material

The solid lignin from softwood enzyme hydrolysis was obtained from a commercial bioethanol plant in Finland, with a dry matter content ranging from 55 wt% to 57 wt%. Subsequently, this lignin was dried in an air blast oven at 105 °C for 12 h, followed by grinding using a vibratory disk mill (Retsch RS 100, Germany) at 200 rpm for 1 h. All chemicals and reagents used in this study were obtained commercially and used without further modification.

2.2. Pretreatment of industrial hydrolysis lignin and lignin model compound with acidic and alkaline DESs, and their fast pyrolysis

The acidic and alkaline DESs were meticulously prepared through the combination of lactic acid and choline chloride in a molar ratio of 2:1, generating what is referred to as Lac/ChCl, and by mixing potassium carbonate (K_2CO_3) and glycerol in a molar ratio of 1:5, producing the K_2CO_3/Gly variant. These mixtures were heated at 80 °C with gentle stirring in an oil bath until complete dissolution of the solid chemicals ensued, yielding liquid solutions. Subsequently, 10 g of raw lignin and 15 g of deionized water (DIW) were introduced into the DES, resulting in a final lignin concentration of 3 wt%. The mixture underwent thorough stirring for 16 h at varying temperatures of 80 °C, 100 °C, and 120 °C. To terminate the reaction, 100 ml of ethanol was added, and the resulting dispersion was filtered via vacuum filtration. Following cooling to room temperature, the filtrate was slowly introduced into DIW and allowed to stand. After 24 h, the lignin precipitated in a flaky form within the water solution. This precipitate was isolated through centrifugation at 10,000 rpm for 10 min and subsequently washed with DIW until the supernatant attained neutral pH. Regarding the alkaline DES, the filtrate was acidified to achieve a pH of approximately 2.0 using HCl under ambient conditions before being combined with DIW. All samples were then freeze-dried for a duration of 72 h and subsequently stored within a desiccator for further use. The resulting acidic and alkaline DES-lignin fractions were labeled as LCHL80/100/120 and KGHL80/100/120, respectively. Additionally, a model compound, 2-(2-methoxyphenoxy)-1-(3,4-dimethoxyphenyl)propane-1,3-diol (VG), representative of a $\beta-O-4$ linked lignin dimer, was subjected to treatment in both acidic and alkaline DESs at 100 °C. This treatment explored the reaction mechanism of lignin within DES media. The remaining Lac/ChCl DES liquid can be recycled by removing water using a rotary evaporator. The K_2CO_3/Gly DES liquid was also recycled after separating water and adjusting the DES properties by K_2CO_3 replenishment.

The pretreated and reference hydrolysis lignins underwent pyrolysis using a laboratory-scale pyrolysis apparatus, and the quantification of gas, char, and bio-oil production was determined based on previous studies [21]. Briefly, 0.5 g of lignin sample was loaded into a quartz U–tube. The carrier gas (N_2, $\geq$ 99.999 %) was purged at a flow rate of 10 ml/min throughout the pyrolysis process. When the furnace was heated to the specified temperature of 550 °C, the U–tube with lignin was inserted into the heated zone quickly and pyrolyzed continuously for 8 min. The pyrolysis volatiles were condensed at the U–tube wall. Finally, the U–tube was removed from the furnace and was allowed to cool to ambient temperature under N_2 atmosphere. After adding absolute ethanol to dissolve the condensed liquid product (bio-oil), the solid product (char) was separated by filtration and then recovered. Three duplicate runs were conducted to ensure the repeatability of measurements.

2.3. Characterizations

The chemical composition and structural characteristics of the lignin fractions were thoroughly analyzed using a range of advanced techniques. HPAEC was employed using a Dionex ICS-5000, CarboPac PA20 column from the USA equipped with a pulse amperometric detector [22]. Elemental analysis was carried out using a CHNS/O FLASH 2000 Series instrument from Thermo Scientific in the USA, coupled with a thermal conductivity detector (TCD), Furthermore, XPS was performed using an ESCALAB 250Xi spectrometer from Thermo Fisher Scientific, UK, coupled with a monochromatized Al Kα x-ray source (1486.68 eV) operating at 300 W. FT-IR was conducted at a 4 cm^{-1} resolution with one hundred co-adding scans per sample spanning the spectral range from 4000 to 400 cm^{-1}, using a Nexus-870 instrument from Thermo Nicolet, USA. NMR spectra, including ^{13}C- and ^{31}P NMR [23] were recorded on a Bruker Avance III 400 (9.4 T) spectrometer (Bruker, Germany), as well as 2D HSQC-NMR [24] and ^{1}DOSY-NMR [25] were recorded on a Bruker Avance III 600 (14.1 T) spectrometer (Bruker, Germany). The thermochemical properties of lignin fractions were investigated using a thermogravimetric analyzer with temperatures ranging from 38 °C to 800 °C under a nitrogen atmosphere employing a Netzsch STA 449F3 instrument from Germany. Additionally, a pyrolyzer (Pyrola 2000, Pyrolab, Sweden) connected with gas chromatography-mass spectrometry was utilized incorporating a 7890B GC system, and an 8977B MSD (Agilent, USA)[26]. The EPR spectra were obtained using a Bruker EMX-10/12 spectrometer (Bruker, Germany) operating at the X-band frequency of 9.82 GHz with a 100 kHz modulation [21]. Comprehensive details of all analytical methods can be found in supporting information.

2.4. Computational study

The simulation of interactions between the lignin model compound and DESs was performed using an MD method in the xTB program to generate thousands of initial configurations of both acidic and alkaline DESs association with guaiacylglycerol–β–guaiacyl ether (GGE) monomer [27]. The clusters generated were preoptimized using the GFN0-xTB level and subsequently at the GFN2-xTB level [28] through the Molclus software package [29]. These resultant clusters were reoptimized at the B3LYP-D3(BJ)/6–31 g* level using Gaussian 16 software package, and it was confirmed that no imaginary frequency appears at this level. Single-point energies for all the optimized conformations were recalculated at the PWPB95-D3/def2-TZVP level using ORCA 4.2.1 software package [30]. The relative energies of the conformations with the lowest energy were calculated using Molclus software. For investigating the non-covalent interactions (NCI) between the optimized DESs and GGE complexes, the independent gradient model based on Hirshfeld partition (IGMH) method [31] was employed using the Multiwfn 3.8 (dev) program [32]. Interaction energy was calculated at M06-2X-D3/ma-TZVP level with the counterpoise method using ORCA 4.2 software package. The visualization of NCI and configuration was carried out using the VMD program [33].

3. Results and discussion

3.1. Simulation of lignin model compound behavior in acidic and alkaline DES pretreatments

Solubility forms the cornerstone for the efficient pretreatment of lignin within a liquid medium. To elucidate the solubility behavior of hydrolysis lignin in both acidic and alkaline DESs, theoretical simulations were employed to explore the potential dissolution mechanisms at the molecular level. The *erythro* isomer of GGE monomer was selected as the lignin model compound [34], because among the complex internal linkages the *erythro* stereostructures of the β–O–4 structures are dominant in natural lignin macromolecules. The structural configuration of GGE is shown in supporting information (Fig. S1). The independent gradient model based on IGMH was used to describe electron density gradient, facilitating the examination of intermolecular and intramolecular NCI between the lignin model compound and DESs (Fig. 2). As depicted in isosurfaces (see Fig. 2a), robust hydrogen bonding (O···H)

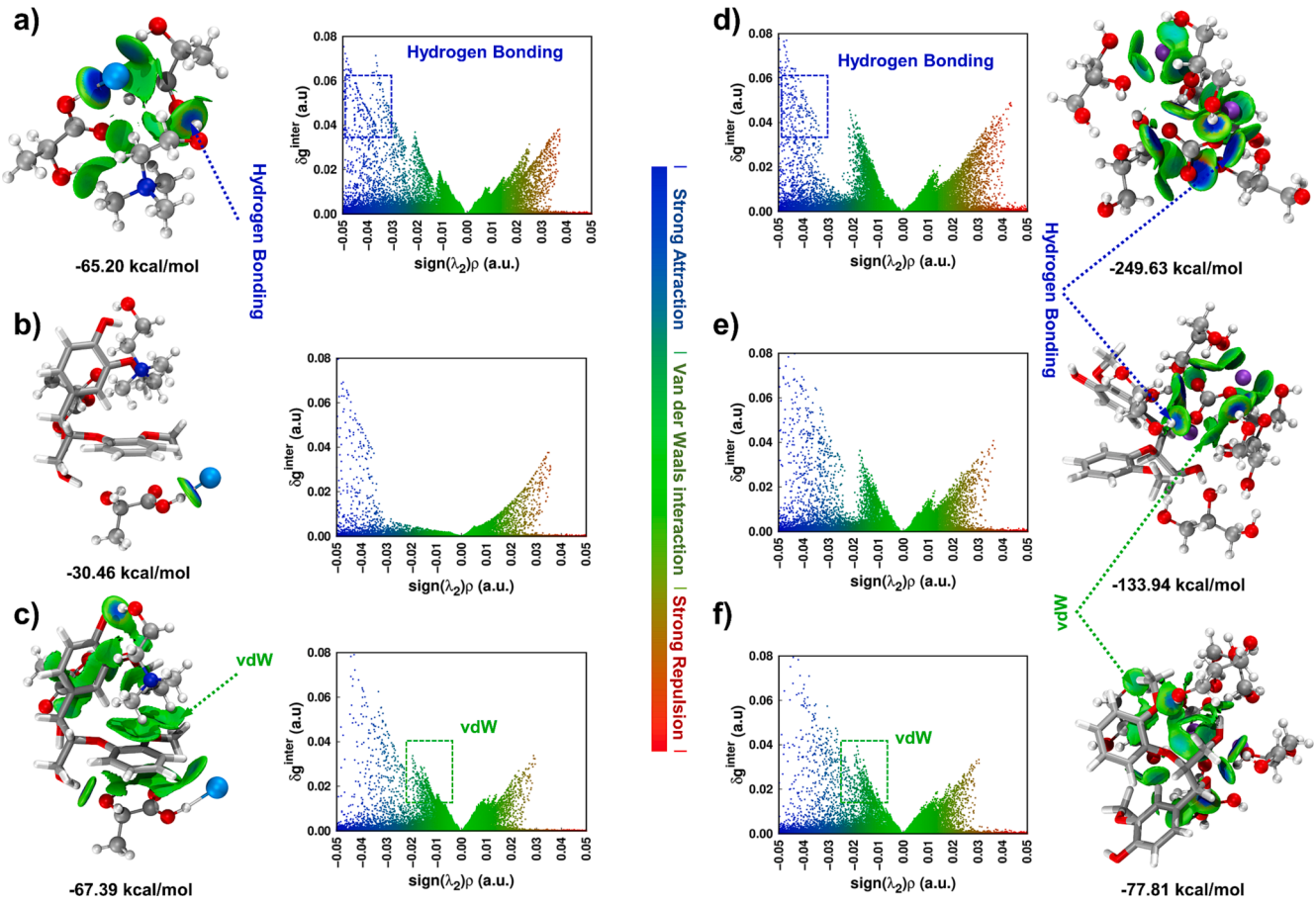

Fig. 2. Scatter graph and isosurface (value = 0.005 electrons/Bohr^3) of the independent gradient model based on the IGMH. These visualizations unveil interactions, including hydrogen bonding and van der Waals (vdW) forces. Panel (a–c) represents the interactions between Lac and ChCl within acidic DES, both in the presence and absence of the lignin model compound (GGE). Panel (d–f) illustrates interactions involving K_2CO_3 and Gly, with and without the presence of GGE. The color scheme is as follows: C (gray), N (blue), H (white), O (red), and Cl (cyan). (For interpretation of the references to color in this figure legend, the reader is referred to the web version of this article.)

interactions were observed between ChCl and Lac molecules in the acidic DES, accompanied by an energy of − 65.20 kcal/mol. The presence of GGE resulted in a reduction of the hydrogen bonding interaction between ChCl and Lac (see Fig. 2b), accompanied by significant van der Waals (vdW) interactions emerging, which facilitated the creation of an isosurface between the GGE molecule and the acidic DES solvent, as depicted in Fig. 2c. Similar behavior was identified between K_2CO_3 and Gly in alkaline DES (see Fig. 2d–f). Indeed, the hydrogen bonding and vdW interactions prove more robust in the alkaline DES compared to the acidic DES. The energy of the vdW interaction remains substantial at 133.94 kcal/mol, even with the introduction of the GGE molecule. Consequently, the viscosity of the alkaline DES surpassed that of the

Table 1
Chemical and elemental composition, C_9 formula, and molar mass of the original lignin (SEHL00), as well as the lignins pretreated with Lac/ChCl (LCHL80–120) or K_2CO_3/Gly (KGHL80–120) DES.

Sample	Composition (wt%)		Elements (wt%)					Molar mass (g/mol)		
	Total lignin[a]	Carbohydrates[b]	C	O	H	N	C_9 formula	$\bar{M}_w$[c]	$\bar{M}_n$[d]	PDI[e]
SEHL00	80.34	14.90	62.75 ±0.16	28.25 ±0.19	5.81 ±0.04	0.53 ±0.00	$C_9H_{9.999}O_{3.039}$	16,821	3268	5.15
LCHL80	79.04	14.04	62.75 ±0.11	29.70 ±0.54	5.79 ±0.08	0.50 ±0.02	$C_9H_{9.965}O_{3.195}$	9701	2981	3.25
LCHL100	80.51	12.46	62.68 ±0.19	30.06 ±0.15	5.77 ±0.02	0.49 ±0.01	$C_9H_{9.942}O_{3.237}$	4670	2946	1.58
LCHL120	79.19	13.03	62.59 ±0.07	30.88 ±0.69	5.74 ±0.02	0.48 ±0.01	$C_9H_{9.904}O_{3.330}$	3763	2801	1.44
KGHL80	90.67	7.68	65.05 ±0.03	28.15 ±0.36	5.78 ±0.01	0.49 ±0.00	$C_9H_{9.596}O_{2.921}$	10,933	4233	2.58
KGHL100	91.46	6.75	65.46 ±0.31	28.11 ±0.09	5.75 ±0.01	0.44 ±0.00	$C_9H_{9.487}O_{2.898}$	5320	3773	1.41
KGHL120	90.79	6.84	65.08 ±0.16	27.79 ±0.13	5.73 ±0.01	0.39 ±0.00	$C_9H_{9.509}O_{2.882}$	3990	2981	1.34

[a] Total lignin: Sum of acid-soluble lignin (ASL, wt%) and acid-insoluble lignin (AIL, wt%) minus ash content (wt%), [b]Total yield of monosaccharides, [c]$\bar{M}_w$: weight-average molecular weight, [d]$\bar{M}_n$: number-average molecular weight, [e]PDI: polydispersity index, the ratio of $\bar{M}_w$ to $\bar{M}_n$.

acidic DES after GGE addition [35]. In summary, the simulations demonstrated that both acidic and alkaline DESs effectively attenuate the hydrogen bonding interaction and π–π stacking within GGE molecules, crucially influencing the structural reforming reactions of lignin within these media.

3.2. Pretreatment of industrial hydrolysis lignin with acidic and alkaline DESs

Laboratory-scale experiments were conducted to elucidate the compositional changes in industrial enzyme-hydrolyzed lignin during acidic or alkaline DES pretreatments (see Fig. 1). Table 1 presents the total lignin content and the carbohydrate contents of raw lignin as well as lignins pretreated with Lac/ChCl or K_2CO_3/Gly DES.

Table 1 shows the content of total lignin (acid soluble and insoluble lignin, i.e. ASL and AIL), and total carbohydrate contents of raw lignin and lignins pretreated with Lac/ChCl or K_2CO_3/Gly DES. The untreated lignin sample (SEHL00) displayed a relatively high lignin content (~80.4 wt%), aligning with the typical value found in industrial lignins (80–90 wt%)[36,37]. However, a significant amount of carbohydrate residues (~15.4 wt%) was also detected, with glucose as the primary monosaccharide, followed by mannose and xylose (Table S1). This relatively high level of polysaccharides likely originated from non-hydrolyzed cellulose and lignin–carbohydrate complexes formed during bioethanol production via enzymatic hydrolysis. The yield of Lac/ChCl DES-lignin ranged from 92.8 wt% to 93.2 wt% and it was much higher than that of K_2CO_3/Gly DES-lignin (from ~ 87.8–88.0 wt%). Thus, there was a larger mass loss of lignin processed in the alkaline DES medium. All the DES-pretreated hydrolyzed lignins (DESLs) showed an increase in total lignin content (from ~ 79 to 91 wt%) and a reduction in residual monosaccharides (from ~ 14.0 down to 6.8 wt%). Particularly noteworthy was the efficient degradation of residual polysaccharides by the alkaline K_2CO_3/Gly DES pretreatment, leading to a substantial decrease in carbohydrate impurities by around 7.2–8.1 wt% and an increase in total lignin content by around 10.3–11.1 wt%. The glucose percentage remained nearly constant after acidic DES pretreatment, indicating that Lac/ChCl DES had only a minor impact on the solubility of unhydrolyzed cellulose. The xylose and mannose contents in lignins decreased from 0.21 wt% and 0.47 wt% to less than 0.1 wt%, underscoring the effective disruption of the lignin–carbohydrate linked by the DES systems. Notably, the pretreatment temperature did not significantly affect the efficiency of DES pretreatments. Overall, the reduction in the content of residual carbohydrates in both DES pretreatments was substantially compared favorably to previously reported DES methods [38,39].

The elemental content of C, H, N, and O in the original lignin and DES-pretreated lignins is presented in Table 1. These values were subsequently used to approximate molecular formulas of the lignin structures based on C_9. Notably, the carbon content of lignin pretreated with acidic DES did not exhibit significant differences, while the oxygen content showed slight increases at rates of 4.9 % (LCHL80), 6.4 % (LCHL100) and 9.3 % (LCHL120) respectively. This phenomenon was likely caused by the cleavage of $C_\beta - O$ within $\beta - O - 4$ substructures to form Hibbert's ketone substituent structures with $C_\beta = O$ (as observed by HSQC-NMR) under acidic reaction system, leading to an enrichment of oxygen. Additionally, it is possible that lignin molecules underwent reduced dehydration during Lac/ChCl DES-induced depolymerization, thereby hindering the cracking of hydroxyl groups [37]. The higher C wt % and lower O wt% observed in KGHL were attributed to the effective removal of carbohydrates aligned with the purity results. In addition, the K_2CO_3/Gly DES pretreatment proved more adept at eliminating N impurities from raw lignin. A notable characteristic of all hydrolysis lignins was their low sulfur content (see Table S1), making the pyrolysis process more straightforward than sulfur-containing lignin grades such as Kraft lignin [40]. Since the contents of other inorganic elements were exceedingly low in all samples (ranging from 0.478 to 0.001 mg/g, Table S1), their potential effects on the lignin pyrolysis process were not further considered.

3.3. Molecular structure of industrial hydrolysis lignin and DES-pretreated lignins

The molecular structure of the original lignin and DES-prtreated lignin fractions was subjected to further analysis using FT-IR spectra (see Fig. 3a) that underwent multiplicative scattering correction. The significant peaks are comprehensively detailed in Table S2. The broad and intense band in the 3600–3200 cm^{-1} range was attributed to the stretching vibrations of the aliphatic and phenolic hydroxyl groups as well as adsorbed water participating in hydrogen bonds. This band exhibited greater breadth and intensity in LCHL compared to KGHL, indicating a relatively more diverse hydrogen bonding system in LCHL. The intensity of this band increased with elevated reaction temperature, revealing the pronounced formation of hydroxyl groups within the lignin structure. The higher hydroxyl content in LCHL was likely a consequence of the substantial cleavage of $\alpha -$ and $\beta - O - 4$ linkages. Notable disparities in the spectra between LCHL and KGHL were observed in the carbonyl region (1800–1600 cm^{-1}, Fig. 3a). In KGHL, the band at around 1710 cm^{-1} indicated the presence of the unconjugated C = O bonds in the side chains of lignin (e.g., ketones, carbonyl and ester groups). The intensity of this band in LCHL far exceeded that in KGHL, and it even shifted to a higher wavenumber (~1740 cm^{-1}). This shift was likely due to the formation of β–ketone carbonyl groups originating from Hibbert's ketone structure in LCHL, suggesting a more pronounced rupture of β–O–4 bonds under Lac/ChCl DES pretreatment [41]. Additionally, the band assigned to the conjugated C = O stretching appeared at 1667 cm^{-1} in LCHL and nearly disappeared in KGHL because of the reduction or degradation of C_α double bonds links (C_α = O), leading to the disruption of the conjugated structure [42]. All lignins exhibited similar characteristics bands in the aromatic vibrational region (bands at 1596, 1513, and 1422 cm^{-1}). Furthermore, signals assigned to guaiacyl (G) units of lignins were detected, specifically the bands at 1266 cm^{-1} and 1211 cm^{-1} associated with the G ring, showing C = O and C − O stretching, respectively, and the peak at 1152 cm^{-1} related to aromatic C − H in-plane deformation, which was also consistent with the typical softwood lignin [43].

The $\bar{M}_w$ and $\bar{M}_n$ of the lignin fractions (Table 1) were determined based on acetylated lignins using DOSY-NMR analysis [25]. The corresponding molar mass distributions are depicted in Fig. 3b. The molar mass of untreated lignin was notably high ($\bar{M}_w \approx 10^4$ g/mol), which aligns with values reported in the literature [44]. However, the $\bar{M}_w$ and $\bar{M}_n$ of DESLs underwent significant alteration, with a decrease of approximately 42 % for LCHL80, 72 % for LCHL100, 77 % for LCHL120, 35 % for KGHL80, 68 % for KGHL100, and 76 % for KGHL120. Consequently, the interconnections between lignin subunits were considerably disrupted, particularly involving the breakage of β–aryl ether bonds within lignin structures, as indicated by NMR results. The $\bar{M}_w$ of both DES-lignins exhibited a gradual decrease with increased pretreatment temperature. Moreover, the PDIs of all DESLs were notably lower than those of SEHL00, especially when the pretreatment temperature reached 120 °C. Thus, a higher temperature facilitated the dissociation of lignin macromolecule, but also produced a more homogeneous molar mass distribution of the DES-pretreated lignin [45].

The near-surface elemental compositions of the lignins were determined and analyzed based on the XPS spectra (Fig. 3c–h, Fig. S2). Qualitative and quantitative results for each element were obtained from the proportional peak areas in deconvoluted high-resolution spectra (Table S3). The surfaces of the lignin fractions mainly consisted of carbon (C1s) and oxygen (O1s) signals at approximately 286 eV and 533 eV, respectively. Additionally, a minor presence of nitrogen (N 1 s) was observed, consistent with the results of the elemental analysis. The atomic concentration ratio of O/C, calculated based on the measured peak area intensities of the lignins, was approximately 0.33 ± 0.15. This value is in good agreement with previously published data,

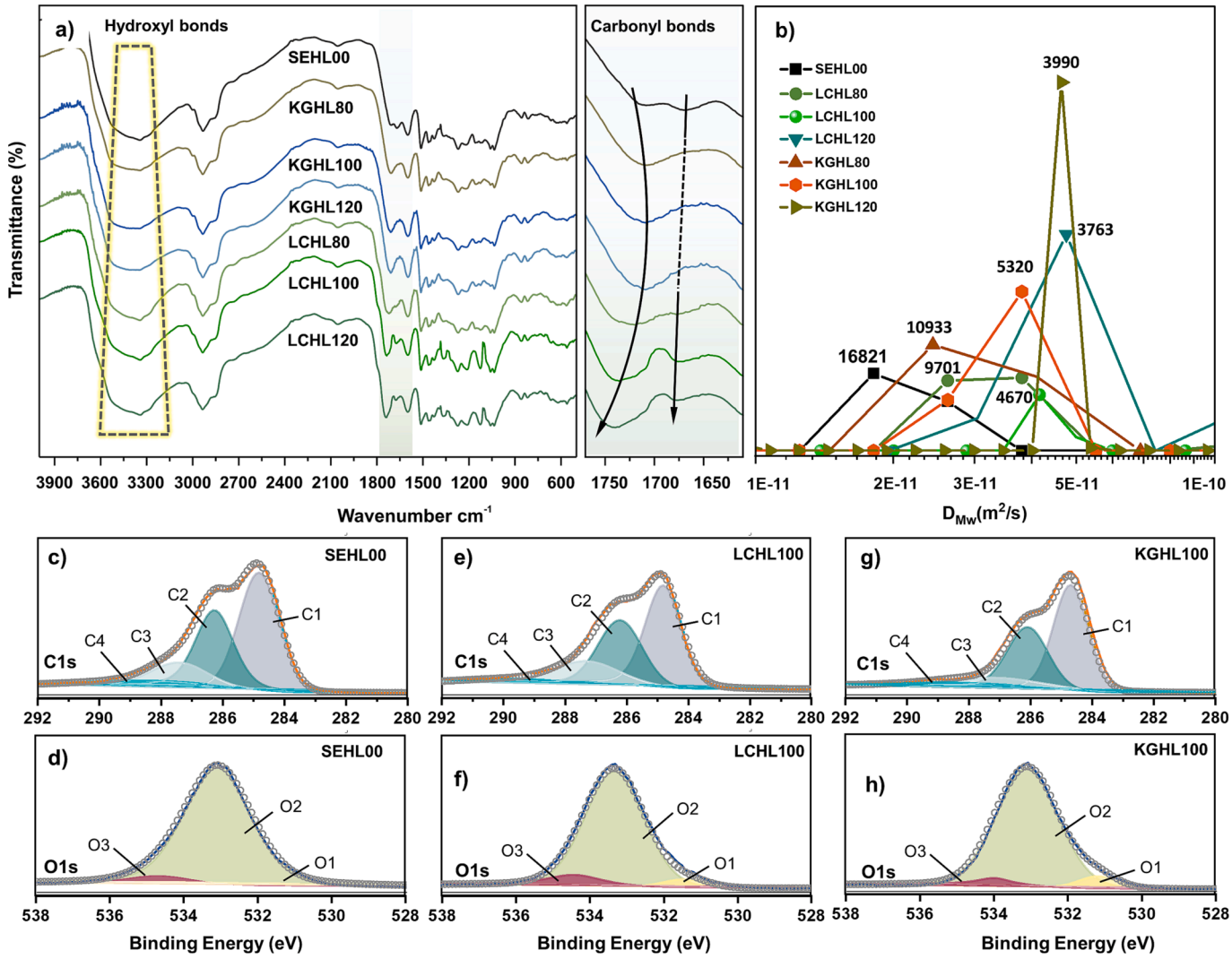

Fig. 3. (a) FT-IR spectra and specific carbonyl bonds patterns, (b) Diffusion coefficient distribution curves determined by DOSY-NMR and corresponding weight-average molecular weights (g/mol), and fitted XPS spectra for C1s and O1s peaks: SEHL00 (c, d), LCHL100 (e, f), and KGHL (g, h).

which indicates that the O/C ratio of pure lignin typically ranges from 0.25 to 0.40, depending on its origin, nature, and sample preparation [46].

Fig. 3 (c–h) presents the deconvoluted high-resolution XPS spectra of the C1s and O1s peaks for raw lignin, LCHL100, and KGHL100. The C1s peak included four carbon components:[47] C − C and C − H (C1), C–O (hydroxyl and ether bonds, C2), C = O and O − C–O (C3), and O − C = O (carboxyl, C4). Additionally, three oxygen components were deconvoluted from the O1s peak:[48] O − C = O and Ar − O − Ar (O1), C − O, C = O, C − O − C and O − C = O (O2), and Ar − OH (O3). The relative proportion of C1 in KGHL was higher than C2, indicating the removal of cellulose contribution [49], suggesting that unhydrolyzed carbohydrates were more easily degraded under K_2CO_3/Gly DES reaction system. The area percentages of C2 and O2 components in DESLs decreased compared to SEHL00, indicating a decrease in ether linkages during pretreatment with DESs. This finding was additionally corroborated by the differences in β–aryl ether bonds as proposed in the HSQC-NMR results. The larger relative area of O3 in LCHL could be explained by the more extensive depolymerization reactions of lignin with Lac/ChCl DES pretreatment, which promoted the generation of phenolic hydroxyl groups, a trend supported by the FT-IR patterns.

The aliphatic hydroxyls (aliphatic–OH), phenolic 5–substituted hydroxyls (G_5–sub.), guaiacyl hydroxyls (G–OH), *p*-hydroxyls (H–OH), and carboxylic acid groups (carboxylic–OH) in all lignin fractions were further analyzed and quantified using ^{31}P NMR spectra (Fig. 4), with the results summarized in Table 2. Aliphatic–OHs were the predominant functional groups in all lignins. Notably, SEHL00 and LCHL exhibited strong signals in this region, potentially overlapping with the –OH signals from carbohydrate impurities, as indicated by a distinct small peak at around 145.8 ppm, which was barely observed in KGHL. The reduced intensity of aliphatic–OH in KGHL suggested that more extensive dehydration and acylation reactions occurred in the lignin side chain, resulting in increased saturated aliphatic segments [45], a trend supported by FT-IR analysis. However, the number of carboxylic–OH groups displayed an opposite trend, suggesting the generation of more decomposed acid functional group-containing structures under K_2CO_3/Gly DES pretreatment compared to Lac/ChCl DES preprocessing. The broad peak centered at 139.8 ppm originated from G–OHs. Remarkably, the amount of G–OH in LCHL was significantly higher than that in KGHL, primarily due to the pronounced dissociation of *β*–O–4 ether linkages during Lac/ChCl DES pretreatments, a topic further discussed in the context of HSQC-NMR analysis. The total phenolic hydroxyl content increased with higher pretreatment temperatures, likely attributed to the severing of *α*– and *β*– aryl ether linkages. Signals in the range of 144.5 to 140.5 ppm correspond exclusively to G_5–substituted units, given that softwood lignin primarily consists of guaiacyl and *p*-hydroxyphenyl units, usually without syringyl units [50].

The higher content of G_5–substituted hydroxyls in KGHL indicated

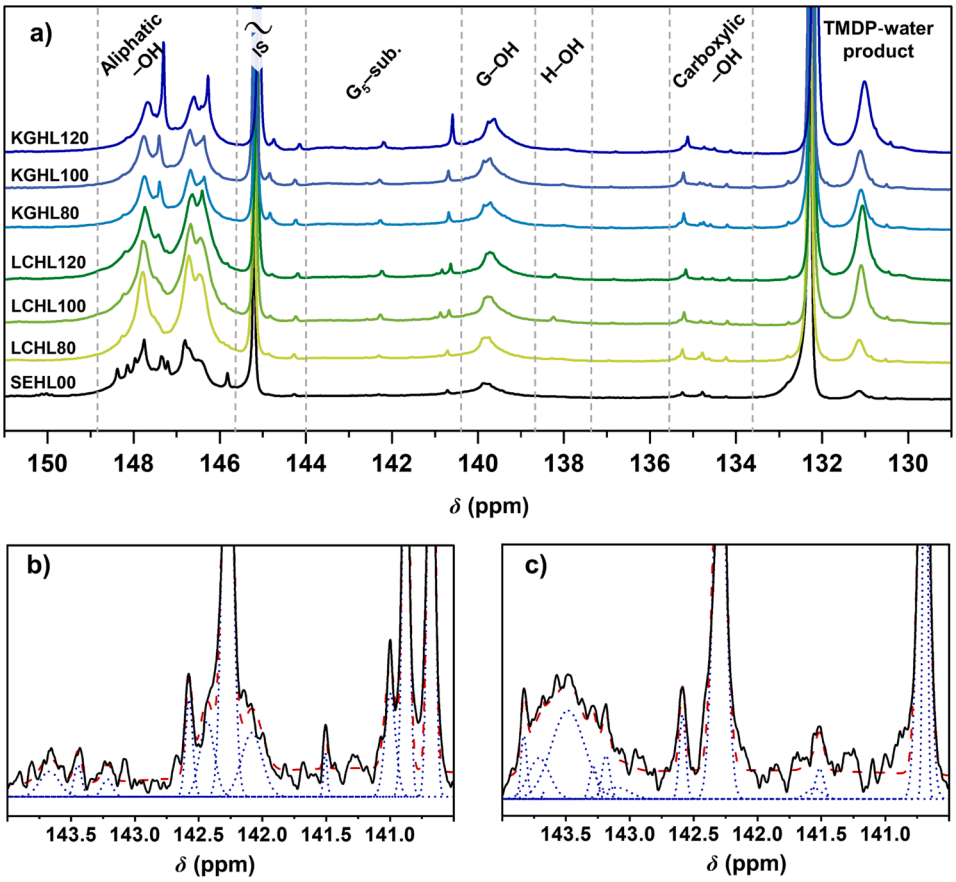

Fig. 4. (a) ^{31}P NMR spectra of phosphorylated lignins and deconvolution of condensed hydroxyl regions in (b) LCHL100 and (c) KGHL100.

Table 2
Contents of various hydroxyl groups (mmol/g) in both original lignin and the lignins subjected to DES pretreatments were determined using ^{31}P NMR spectra.

Samples	Aliphatic–OH	Phenolic–OH				Carboxylic–OH
		Condensed G_5–sub.	Noncondensed G–OH	H–OH	Total –OH[a]	
SEHL00	3.65	0.56	0.63	0.11	1.30	0.24
LCHL80	3.15	0.55	0.61	0.08	1.24	0.16
LCHL100	3.41	0.53	0.70	0.12	1.35	0.16
LCHL120	3.24	0.55	0.83	0.15	1.53	0.17
KGHL80	1.88	0.40	0.40	0.07	0.87	0.14
KGHL100	1.85	0.57	0.59	0.09	1.25	0.22
KGHL120	2.13	0.60	0.63	0.11	1.34	0.23

[a] Total–OH content is calculated from the formula: Total–OH = condensed G_5–sub. + G–OH + H–OH.

more condensed structures linked to the 5–position of aromatic carbon, implying that K_2CO_3/Gly DES pretreatment induced more condensation reactions. The small peak at around 138.4 ppm corresponded to H subunits (H–OH). However, more H–OH was present in LCHL, suggesting the degradation of guaiacyl-type structures to *p*-hydroxyphenyl-type structures due to the destruction of methyl aryl ether bonds through acidic DES pretreatment [51].

The structural characterization of the acetylated lignin fractions involved 2D HSQC-NMR analysis, which allowed for the identification of interlinkage changes resulting from the Lac/ChCl and K_2CO_3/Gly DES pretreatments compared to the untreated hydrolysis lignin. The correlation cross-signals were assigned using established references from previous studies [42,52–54], as detailed in Table S4. The relative abundance of interunit linkages and functional groups was estimated by integrating the corresponding correlated contours within the HSQC spectra. The aromatic G_2 signals were used as the lignin reference in this assessment. To be precise, the HSQC spectra corresponding to the aliphatic side chains of the lignins (Fig. 5, δ_C/δ_H 45–105/2.5–5.5 ppm) indicated that the primary interlinkages in all lignin fractions were alkyl–aryl ethers (β–O–4, A), followed by resinol (β–β, C) substructures. A noticeable reduction in the relative abundance of β–O–4 linkages was observed in DESLs compared to the untreated lignin, and this reduction became more pronounced with the increase in preprocessing temperature. This observation indicates that the lignin macromolecules underwent depolymerization and degradation during DES pretreatments, resulting in a significant decrease in the number of β–O–4 linkages.

The notable reduction in β–O–4 linkages within monolignols corresponded with the decrease in the molar mass ($\bar{M}_w$), as indicated in Table 1. Furthermore, the β–β content in LCHL and KGHL experienced only a marginal decrease, implying that the influence of DESs on the carbon–carbon linkages within the untreated lignin was relatively minor. Alongside these primary interunit linkages, the presence of Hibbert's ketone (HK) substructure was confirmed by the appearance of C_α–H_α cross-peak at 68.19/5.01 ppm. Notably, this peak signal was

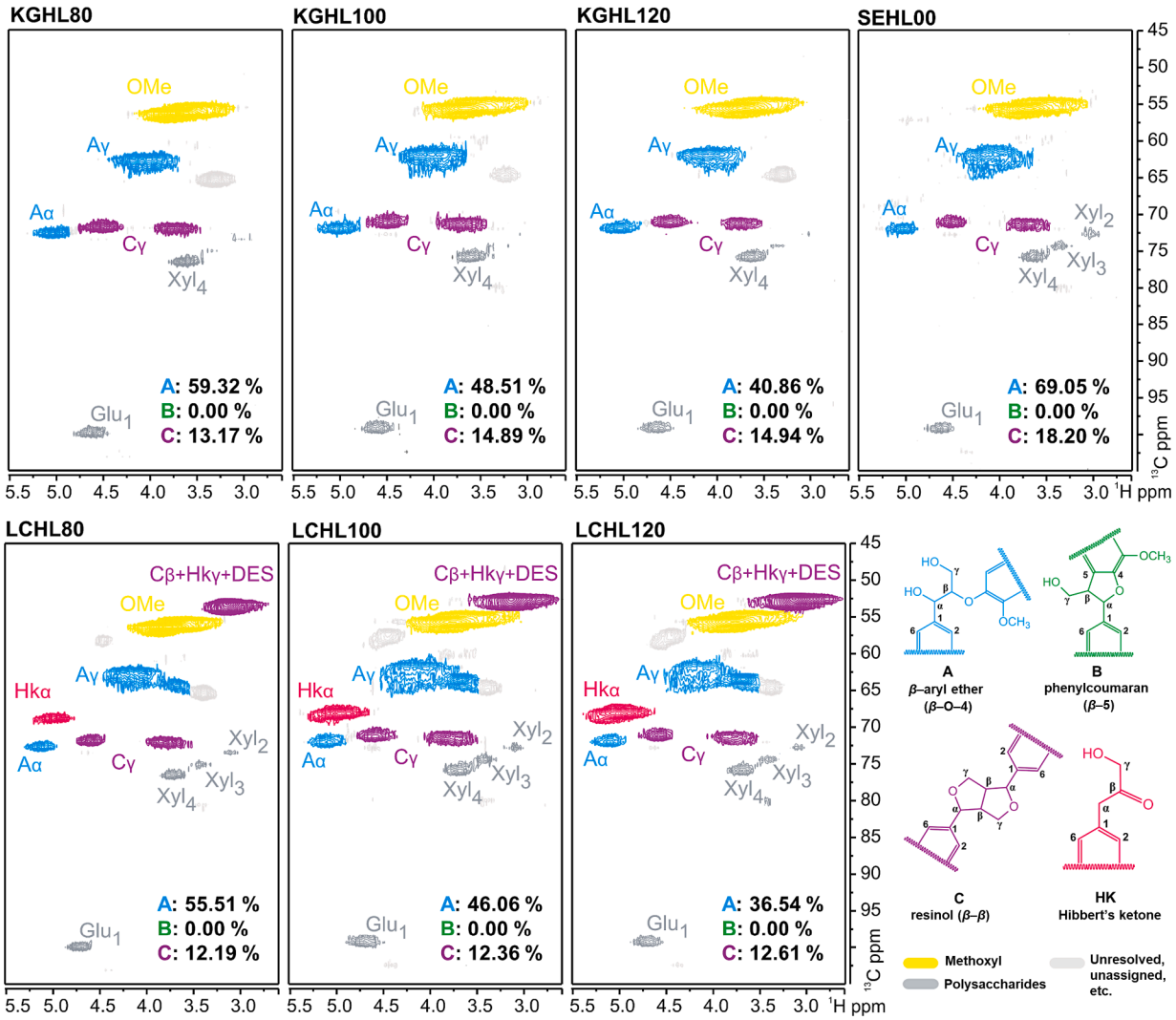

Fig. 5. Partial aliphatic regions from HSQC-NMR spectra of untreated lignin and DES-pretreated lignins post-acetylation. The contours representing lignin substructure units are color-coded. The relative content of the predominant aliphatic interunit was determined through contour integration.

exclusively observed in LCHL. The disappearance of partial ether bonds coincided with the formation of HK substructures, providing direct evidence for unimpeded depolymerization of raw lignin during Lac/ChCl DES pretreatment. Additionally, two carbohydrate-lignin complex linkages, xylan-lignin (Xyl) and glucan-lignin (Glu), were identified and characterized. A lower intensity of glucan- and xylan-related cross-signals was evident in KGHL, indicating a more extensive removal of residual carbohydrates during K_2CO_3/Gly DES preprocessing. The peaks associated with the aromatic ring units of lignins (Fig. S3, δ_C/δ_H 105–150/6.0–8.5 ppm) revealed that the hydrolysis lignin primarily consisted of guaiacyl (G) units with a minor presence of *p*-hydroxyphenyl units (H). This composition aligns with the characteristics of the raw material (that is, softwood sawdust), and no significant differences were observed among the various samples.

The potential reaction mechanisms for lignin depolymerization in Lac/ChCl and K_2CO_3/Gly DES pretreatments are depicted in Fig. 6. The predominant linkage, *β*–O–4 substructure, underwent decomposition in both acidic and alkaline DESs. However, the reaction pathways leading to the cleavage of these *β*–O–4 bonds differed significantly. Lignin subjected to Lac/ChCl DES pretreatment resulted in substructures primarily characterized by Hilbert's ketones, while the K_2CO_3/Gly DES pretreatment was likely to promote the formation of benzyl ketones and aldehydes.

The chemical interlinkages of the lignin fractions were further elucidated through ^{13}C NMR (see Fig. S4). Semi-uantitative data on interunit bonds for raw and DES-pretreated lignins were obtained by integrating the ^{13}C NMR spectra, as outlined in Table 3. The integral value of the ^{13}C NMR spectral region at δ160–103 ppm was employed as a reference for quantifying the lignin interlinkages, specifically corresponding to the six aromatic carbons [55]. The data revealed insignificant variations in the amount of methoxy groups among the studied lignins. The aromatic region was divided into three segments: oxygenated aromatic region carbons ($C_{Ar–O}$, 160–141 ppm), condensed aromatic region carbons ($C_{Ar–C}$, 141–125 ppm), and protonated aromatic region carbons ($C_{Ar–H}$, 125–103 ppm). The degree of condensation (DC) was estimated by subtracting the integral of the $C_{Ar–H}$ region from 3, based on the assumption that uncondensed softwood lignin possesses three aromatic protons at the CH-2, CH-5, and CH-6 positions [56]. The results indicated that the DC values of KGHL were slightly higher than those of LCHL. Furthermore, the DC of DESLs remained relatively consistent under 80 °C and 100 °C reaction conditions compared with the original lignin, but it notably increased under 120 °C. This phenomenon was attributed to condensation reactions occurring at high temperatures on the 2-, 5-, or 6-positions within the aromatic units of lignin [56,57].

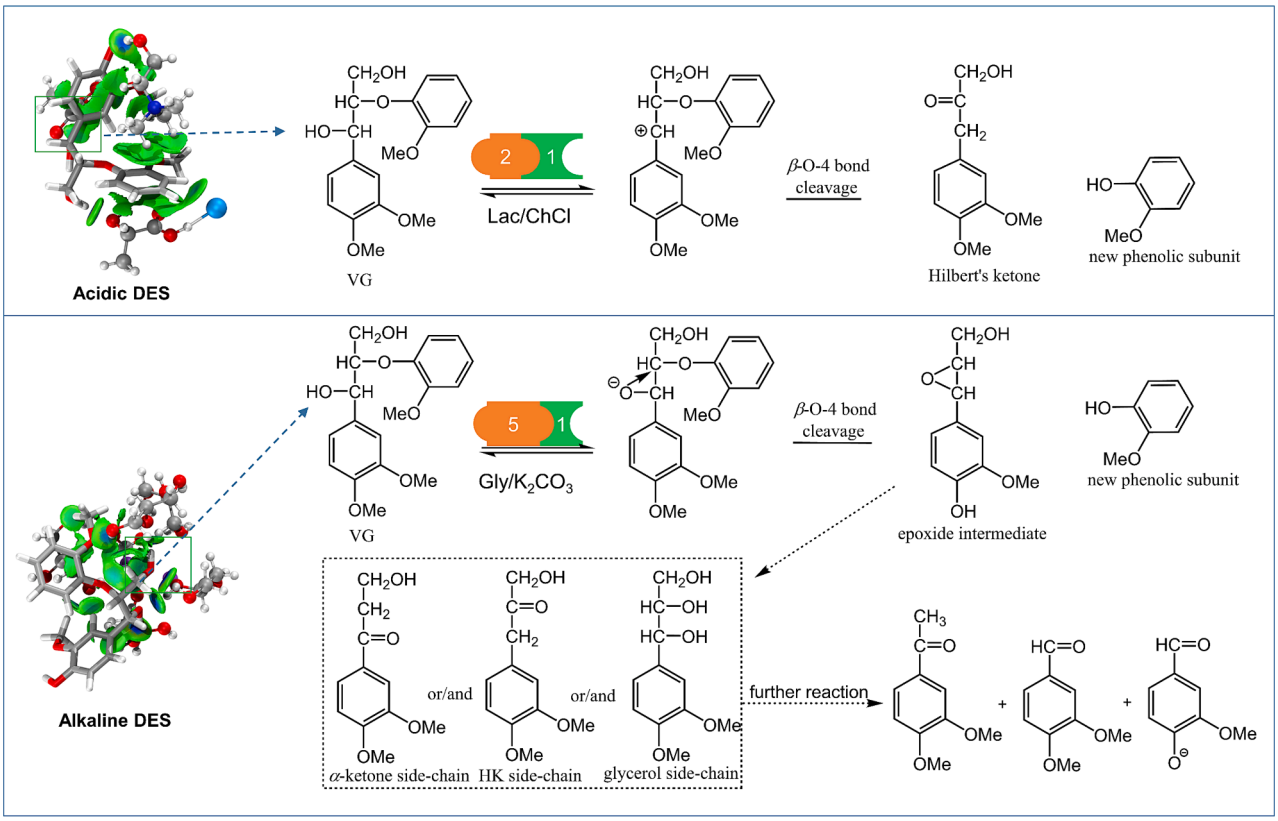

Fig. 6. Reaction pathways for lignin model compound (VG) in acidic and alkaline DESs. (a) In the presence of acidic DES (with ChCl as the HBA and HBD), the initial step involves the cleavage of the β–O–4 linkage, subsequently leading to the formation of Hilbert's ketone. (b) Conversely, when alkaline DES (K_2CO_3 as HBA and Gly as HBD) the process begins with the β–O–4 cleavage, followed by the creation of benzyl ketone and aldehyde structures.

Table 3
Semi-quantitative assessment of structural interlinkages abundance in the initial lignin and DES-pretreated lignins evaluated through ^{13}C-NMR[a].

lignin interunit bonds	/Ar SEHL00	LCHL80	LCHL100	LCHL120	KGHL80	KGHL100	KGHL120
CH_3O	0.85	0.90	0.92	0.95	0.85	0.89	0.92
C_{Ar-H}	2.26	2.26	2.24	2.12	2.22	2.19	2.07
C_{Ar-C}	1.95	1.96	2.02	2.10	2.03	2.05	2.21
C_{Ar-O}	1.79	1.78	1.74	1.78	1.75	1.76	1.72
Degree of condensation[b]	0.74	0.74	0.76	0.88	0.78	0.81	0.93

[a]The integration of δ160–103 ppm (6.0) was employed as the internal standard for quantification, and the quantities of aromatic carbon linkages are expressed as a count per aromatic ring (/Ar). [b]Calculated from 3 minus the integral value for C_{Ar-H} region.

3.4. Thermal behavior and fast pyrolysis of industrial hydrolysis lignin and DES-pretreated lignins

The thermochemical stability and thermal degradation characteristics of SEHL00 and DESLs were investigated through thermogravimetric analysis including thermal gravimetry (TG) and derivative thermal gravimetry (DTG) analysis. Fig. 7a illustrates the TG and the corresponding DTG profiles of the original and DES-pretreated lignins, while more detailed data is presented in Table S5. Within the TG curves of all lignins, a gradual decline appeared within the 40 °C–150 °C range, indicating minimal moisture evaporation from the lignin fractions during the heating (approximately 0.83–1.19 wt%). The minor shoulder observed between 150 °C and 280 °C resulted from the presence of carbohydrate impurities, small molecular lignin degradation, and weaker C − O bonds within the β − O − 4 linkages [58]. The shoulder peaks of LCHL occurred at higher temperatures compared to those of KGHL. This discrepancy likely arose from the higher residual hydrolyzed sugar content in lignin prepared with Lac/ChCl DES along with the more heterogeneous molar mass distribution. Furthermore, LCHL exhibited fewer β − O − 4 aryl ether bonds. Extensive decomposition of all lignins took place within the 280 °C–600 °C range, releasing volatiles stemming from lignin degradation due to the cleavage of thermally unstable linkages. Notably, the maximum mass loss rate (R_{max}) for LCHL increased by approximately 0.15 %/°C when compared to SEHL00. Conversely, KGHL displayed a reduction of approximately 0.1 %/°C in R_{max}. Intriguingly, the temperatures corresponding to R_{max} for all DESLs were elevated by over 10 °C, where the decomposition temperature of LCHL was slightly higher than that of KGHL. It is likely that DES pretreatments augmented the thermal stability of lignin, potentially due to the disruption of β − O − 4 linkages possessing the lower bond dissociation energies. Comparatively, the degradation residue (char) content of LCHL was significantly lower than that of SEHL00. In contrast, the K_2CO_3/Gly DES pretreatment led to an increased formation of decomposed residue (~5 wt%), indicating a heightened degree of lignin condensation to char during high-temperature pyrolysis.

The chemical attributes of lignin pyrolysis products were meticulously scrutinized through Py–GC/MS analysis at a rapid pyrolysis temperature of 550 °C. The identification of peaks and the

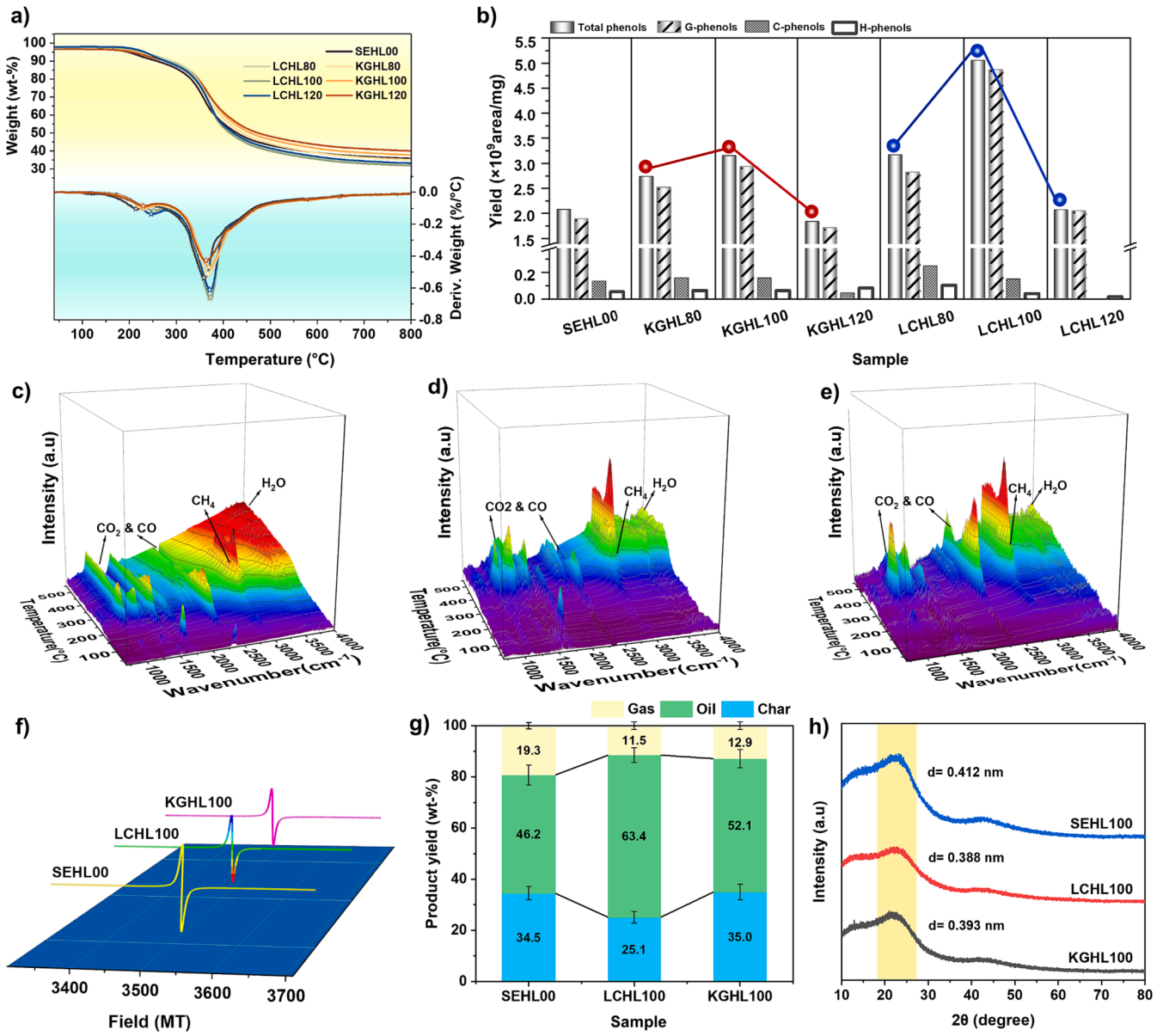

Fig. 7. (a) TG-DTG curves, (b) the distribution profile of primary phenolic products in rapid pyrolysis (c–e) three-dimensional TG-FTIR spectra, (f) sub-curves derived from EPR fitting, (g) gas, oil, and char yields during pyrolysis, and (h) XRD spectra of SEHL00, LCHL100 and KGHL100.

corresponding relative abundances of pyrolysis compounds are concisely compiled in the supporting information (see Table S6). The yields of primary specific phenolic compounds, encompassing guaiacyl-type phenols (G-phenols), catechol-type phenols (C-phenols), and *p*-hydroxylphenyl-type phenols (H-phenols), along with the overall phenolic compounds, originating from initial lignin and DES-pretreated lignins (SEHL00 and DESLs), are delineated in Fig. 7b. The semi-quantitative comparative analysis of pyrolytic compound yields was executed by normalizing the peak area to the sample loading mass. Both the acidic and alkaline pretreatments bolstered the thermal decomposition of hydrolysis lignin into phenolic products, with corresponding normalized peak areas of 3.16×10^9 and 5.05×10^9 for acidic DES pretreatments, while 2.72×10^9 and 3.14×10^9 for alkaline DES pretreatments, at reaction temperatures of 80 °C and 100 °C. For context, the normalized peak area of the original hydrolysis lignin stood at 2.05×10^9. As the reaction temperature reached 120 °C, the yields of phenolic products in both LCHL120 and KGHL120 subsided to 2.06×10^9 and 1.82×10^9, respectively. This decline was attributed to lignin condensation at high temperatures, as a deduction supported by 13C NMR results. The capability of DES in facilitating the phenolic compound production has also been reported in other studies, although a decrease in the yield has also been presented [51,59–61].

The phenolic monomers were predominantly constituted of alkoxyphenols featuring a single methoxy group, originating from the G-units within lignin. Among these, 4-methylguaiacol (C_8) exhibited the highest relative abundance, trailed by guaiacol (C_7) and 4-vinylguaiacol (C_9), consistently observed across all lignin samples, as indicated by the GC/MS spectra (see Fig. S5). The collective relative area percentages of these three compounds spanned from 44.6 % to 49.8 % in KGHL, and 40.0 % to 51.5 % in LCHL (in contrast to the 40.0 % observed in raw lignin, as presented in Table S6). The formation of these alkoxyphenolic products resulted from the cleavage of alkyl side chains within the lignin structure [62,63]. The bio-oil enriched in alkoxyphenols exhibits a high utilization potential, e.g., as a substitute for petroleum-based phenol in the synthesis of phenol–formaldehyde resins and in the production of polyurethanes and epoxy resins, in addition to being upgraded in-situ or ex-situ into monoaromatic and naphthenic alkane hydrocarbon fuels by catalysts with tailored properties [64].

The emissions of gases were monitored via TG-FTIR analysis (Fig. 7c–e) to offer further insights into the lignin pyrolysis chemistry, utilizing LCHL100 and KGHL100 lignin fractions. Both DES pretreatments led to a reduction in gas release (H_2O, CO_2, CO, and CH_4) below 300 °C. This decrease was attributed to the diminished number of β–O–4 interlinks, which in turn lowered the production of highly reactive small-molecule free radicals generated from the cracking of ether links [65]. The central reaction pathway in lignin pyrolysis is driven by free radical processes. Notably, the concentration of stable free radicals in lignin biochar has been observed to correlate with the bio-oil yield [66,67]. Therefore, the concentration of free radicals in the residual char was subjected to meticulous analysis. The extracted curves from the experimental EPR spectra and the computational outcomes about free radical concentrations across diverse lignin fractions are illustrated in Fig. 7f and S6. During pyrolysis at 550 °C, the concentration of char free radicals was 3.84 × 10^{17} spin/g for SEHL00, 1.61 × 10^{17} spin/g for LCHL100, and 1.67 × 10^{17} spin/g for KGHL100. This trend was in alignment with the bio-oil yields of SEHL00, LCHL100, and KGHL100, which were 46.2 wt%, 63.4 wt%, and 52.1 wt%, respectively (see Fig. 7g). The structural reconstruction catalyzed by the fragmentation of β–O–4 bonds in DESL impeded the formation of stable free radicals within lignin char. Remarkably, the lowest concentration of free radicals was identified in the residual char of LCHL100. This suggests that effective radical quenching reactions occurred within the radical intermediates generated from lignin fragments, mitigating polymerization and cross-linking reactions. Conversely, the K_2CO_3/Gly DES pretreatment facilitates char formation, likely due to the presence of cross-linked and carbonized structures [68]. The XRD patterns revealed the substantial influence of Lac/ChCl and K_2CO_3/Gly DES pretreatments on residual carbon formation within lignin, resulting in a reduction of the interlayer spacing in carbon [69] (see Fig. 7h).

Pathways and mechanisms underlying the formation of key pyrolysis products were deduced from the pyrolysis data (Fig. 8). The pivotal role of β–O–4 linkages within DESL in shaping the distribution of pyrolysis products from hydrolysis lignin was substantiated. The disruption of β–O–4 bonds, coupled with the consequent rearrangement of molecular units within lignin promoted by DES preprocessing, facilitated the creation of phenolic volatiles and concurrently impeded char formation during pyrolysis. It is noteworthy that the suppressive impact of K_2CO_3/Gly DES on char formation was not highly pronounced.

4. Conclusion

DES pretreatments using acidic Lac/ChCl and alkaline K_2CO_3/Gly DES solvents initiated depolymerization reactions primarily focused on β–O–4 bond cleavage. This phenomenon resulted in a noteworthy decrease in the molar mass of industrial hydrolysis lignin, concurrently augmenting its thermochemical stability. The distinct degradation mechanisms induced by DES pretreatments were evident through differences in lignin structural composition. LCHL displayed more unconjugated carbonyl structures compared to KGHL, while KGHL contained a higher proportion of condensed substitutions incorporating aromatic rings. During pyrolysis, aliphatic side-chain linkages of DES-pretreated hydrolysis lignin underwent cracking, resulting in a substantial generation of phenolic compounds, particularly alkoxyphenols. The total quantity of phenolic compounds and bio-oil yield from acidic DES-lignin surpassed that from alkaline DES-lignin. Notably, the most substantial increase in G-phenol content was observed in both acidic and alkaline DES-lignin prepared at 100 °C showing a remarkable difference in the pyrolytic performance of lignin (increase by a factor of 2.59 and 1.55, respectively). As a result, acidic DES pretreatment holds remarkable potential for the thermal conversion of industrial bioethanol lignin into monophenolics, thus promoting the valorization of residual hydrolysis lignin for bio-based chemicals and materials. Additionally, alkaline DES pretreatment can enhance bio-oil production from lignin.

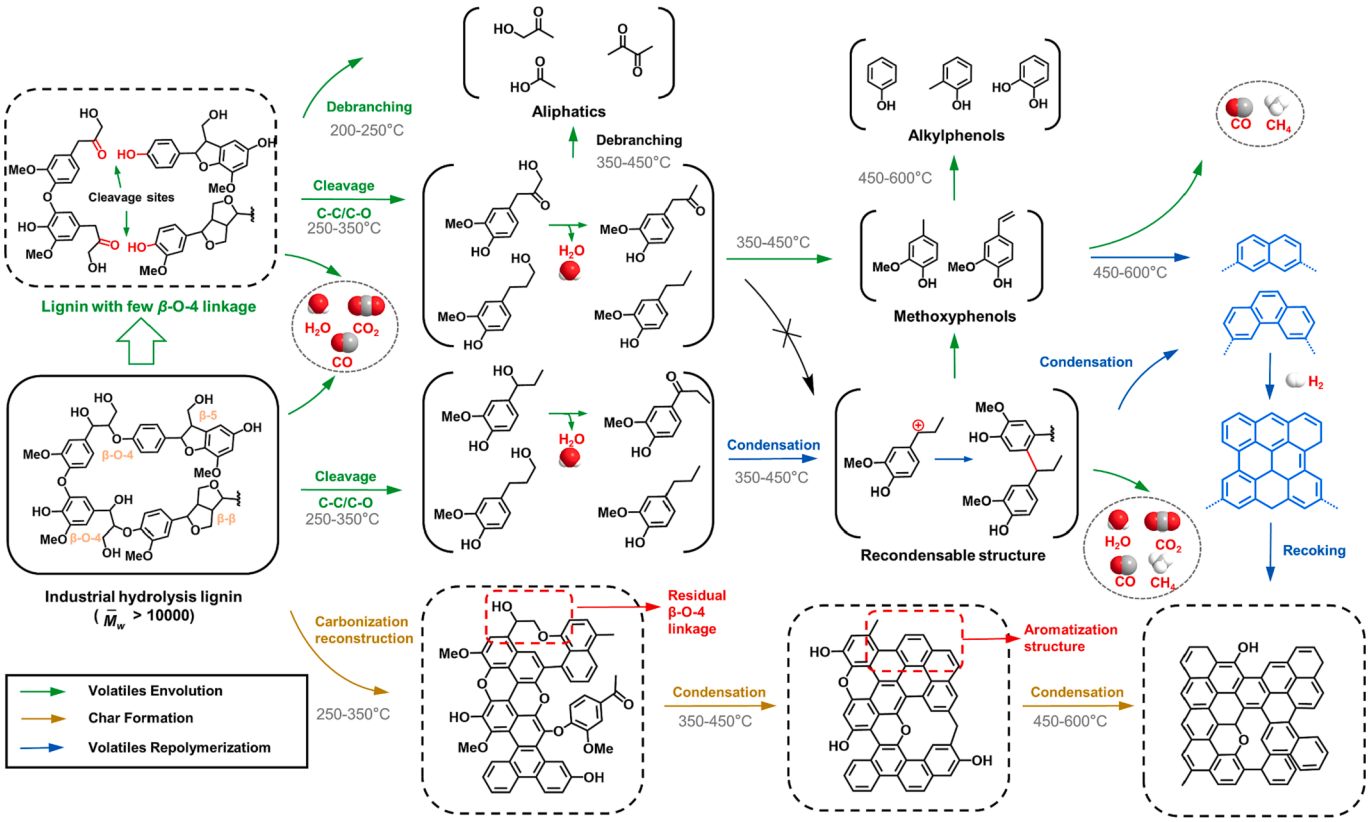

Fig. 8. The proposed reaction pathways for both untreated and DES-pretreated hydrolysis lignin during rapid pyrolysis.

Declaration of Competing Interest

The authors declare that they have no known competing financial interests or personal relationships that could have appeared to influence the work reported in this paper.

Data availability

Data will be made available on request.

Acknowledgements

This work was supported by the China Scholarship Council (grant numbers 201806600040, 201908120132), the Walter Ahlström Foundation Grant (grant number 20230107), BioKainuu project (VN/24008/2021-OKM-1), the European Research Council (grant number 772110), Research Council of Finland (grant numbers 355001, 340099), KAUTE foundation, Finnish Cultural Foundation-Kalle and Dagmar Välimaan Fund, and the National Natural Science Foundation of China (grant number 22208061). Part of the work was carried out with the support of the Centre for Material Analysis and Kvantum Institute at the University of Oulu, Finland. We would like to thank Jasmiini Tornberg for editing the images of graphical abstract and experimental procedure.

Appendix A. Supplementary data

Supplementary data to this article can be found online at https://doi.org/10.1016/j.cej.2023.147368.

References

[1] L.T. Mika, E. Cséfalvay, Á. Németh, Catalytic conversion of carbohydrates to initial platform chemicals: chemistry and sustainability, Chem. Rev. 118 (2) (2018) 505–613.
[2] B.B. Uzoejinwa, X. He, S. Wang, A.-E.-F. Abomohra, Y. Hu, Q. Wang, Co-pyrolysis of biomass and waste plastics as a thermochemical conversion technology for high-grade biofuel production: Recent progress and future directions elsewhere worldwide, Energy Convers. Manage. 163 (2018) 468–492.
[3] H.M. Zabed, S. Akter, J. Yun, G. Zhang, F.N. Awad, X. Qi, J. Sahu, Recent advances in biological pretreatment of microalgae and lignocellulosic biomass for biofuel production, Renew. Sustain. Energy Rev. 105 (2019) 105–128.
[4] S. Chovau, D. Degrauwe, B. Van der Bruggen, Critical analysis of techno-economic estimates for the production cost of lignocellulosic bio-ethanol, Renew. Sustain. Energy Rev. 26 (2013) 307–321.
[5] A. Milovanoff, I.D. Posen, B.A. Saville, H.L. MacLean, Well-to-wheel greenhouse gas implications of mid-level ethanol blend deployment in Canada's light-duty fleet, Renew. Sustain. Energy Rev. 131 (2020), 110012.
[6] R. García, C. Pizarro, A.G. Lavín, J.L. Bueno, Biomass sources for thermal conversion. Techno-economical overview, Fuel 195 (2017) 182–189.
[7] M.V. Galkin, J.S. Samec, Lignin valorization through catalytic lignocellulose fractionation: a fundamental platform for the future biorefinery, ChemSusChem 9 (13) (2016) 1544–1558.
[8] W. Schutyser, a.T. Renders, S. Van den Bosch, S.-F. Koelewijn, G. Beckham, B.F. Sels, Chemicals from lignin: an interplay of lignocellulose fractionation, depolymerisation, and upgrading, Chem. Soc. Rev. 47(3) (2018) 852–908.
[9] I. Brzonova, E. Kozliak, A. Kubátová, M. Chebeir, W. Qin, L. Christopher, Y. Ji, Kenaf biomass biodecomposition by basidiomycetes and actinobacteria in submerged fermentation for production of carbohydrates and phenolic compounds, Bioresour. Technol. 173 (2014) 352–360.
[10] J. Li, X. Bai, Y. Fang, Y. Chen, X. Wang, H. Chen, H. Yang, Comprehensive mechanism of initial stage for lignin pyrolysis, Combust. Flame 215 (2020) 1–9.
[11] E. Liakakou, B. Vreugdenhil, N. Cerone, F. Zimbardi, F. Pinto, R. André, P. Marques, R. Mata, F. Girio, Gasification of lignin-rich residues for the production of biofuels via syngas fermentation: Comparison of gasification technologies, Fuel 251 (2019) 580–592.
[12] Q. Lu, W.-L. Xie, B. Hu, J. Liu, W. Zhao, B. Zhang, T.-P. Wang, A novel interaction mechanism in lignin pyrolysis: Phenolics-assisted hydrogen transfer for the decomposition of the β–O–4 linkage, Combust. Flame 225 (2021) 395–405.
[13] J. Zakzeski, P.C. Bruijnincx, A.L. Jongerius, B.M. Weckhuysen, The catalytic valorization of lignin for the production of renewable chemicals, Chem. Rev. 110 (6) (2010) 3552–3599.
[14] S. Ghosh, S. Das, R. Chowdhury, Effect of pre-pyrolysis biotreatment of banana pseudo-stem (BPS) using synergistic microbial consortium: role in deoxygenation and enhancement of yield of pyro-oil, Energy Convers. Manage. 195 (2019) 114–124.
[15] T. Han, N. Sophonrat, A. Tagami, O. Sevastyanova, P. Mellin, W. Yang, Characterization of lignin at pre-pyrolysis temperature to investigate its melting problem, Fuel 235 (2019) 1061–1069.
[16] B. Zhang, D. Yang, H. Wang, Y. Qian, J. Huang, L. Yu, X. Qiu, Activation of enzymatic hydrolysis lignin by NaOH/urea aqueous solution for enhancing its sulfomethylation reactivity, ACS Sustain. Chem. Eng. 7 (1) (2018) 1120–1128.
[17] J.-Y. Kim, S. Heo, J.W. Choi, Effects of phenolic hydroxyl functionality on lignin pyrolysis over zeolite catalyst, Fuel 232 (2018) 81–89.
[18] S. Li, Z. Luo, W. Wang, K. Lu, Y. Yang, X. Liang, Characterization of pyrolytic lignin and insight into its formation mechanisms using novel techniques and DFT method, Fuel 262 (2020), 116516.
[19] V. Bušić, S. Roca, D. Vikić-Topić, K. Vrandečić, J. Ćosić, M. Molnar, D. Gašo-Sokač, Eco-friendly quaternization of nicotinamide and 2-bromoacetophenones in deep eutectic solvents. Antifungal activity of the products, Environ. Chem. Lett. 18 (2020) 889–894.
[20] N. Ismail, J. Pan, M. Rahmati, Q. Wang, D. Bouyer, M. Khayet, Z. Cui, N. Tavajohi, Non-ionic deep eutectic solvents for membrane formation, J. Membr. Sci. 646 (2022), 120238.
[21] Y. Fan, M. Lei, Z. Zhang, X. Kong, W. Xu, Y. Han, M. Li, C. Liu, R. Xiao, Unmasking radical-mediated lignin pyrolysis after benzyl hydroxyl shielding, Bioresour. Technol. 342 (2021), 125944.
[22] X. Yue, T. Suopajärvi, O. Mankinen, M. Mikola, A. Mikkelson, J. Ahola, S. Hiltunen, S. Komulainen, A.M. Kantola, V.-V. Telkki, Comparison of lignin fractions isolated from wheat straw using alkaline and acidic deep eutectic solvents, J. Agric. Food Chem. 68 (51) (2020) 15074–15084.
[23] A. Brandt, L. Chen, B.E. van Dongen, T. Welton, J.P. Hallett, Structural changes in lignins isolated using an acidic ionic liquid water mixture, Green Chem. 17 (11) (2015) 5019–5034.
[24] C. Alvarez-Vasco, R. Ma, M. Quintero, M. Guo, S. Geleynse, K.K. Ramasamy, M. Wolcott, X. Zhang, Unique low-molecular-weight lignin with high purity extracted from wood by deep eutectic solvents (DES): a source of lignin for valorization, Green Chem. 18 (19) (2016) 5133–5141.
[25] J.R. Montgomery, P. Bazley, T. Lebl, N.J. Westwood, Using Fractionation and Diffusion Ordered Spectroscopy to Study Lignin Molecular Weight, ChemistryOpen 8 (5) (2019) 601–605.
[26] R. Liu, A. Smeds, L. Wang, A. Pranovich, J. Hemming, S. Willfor, H. Zhang, C. Xu, Fractionation of lignin with decreased heterogeneity: based on a detailed characteristics study of sequentially extracted softwood kraft lignin, ACS Sustain. Chem. Eng. 9 (41) (2021) 13862–13873.
[27] S. Spicher, S. Grimme, Robust atomistic modeling of materials, organometallic, and biochemical systems, Angew. Chem. Int. Ed. 59 (36) (2020) 15665–15673.
[28] C. Bannwarth, S. Ehlert, S. Grimme, GFN2-xTB—An accurate and broadly parametrized self-consistent tight-binding quantum chemical method with multipole electrostatics and density-dependent dispersion contributions, J. Chem. Theory Comput. 15 (3) (2019) 1652–1671.
[29] T. Lu, molclus program. http://www.keinsci.com/research/molclus.html. (Accessed 25 March 2023).
[30] F. Neese, Software update: the ORCA program system, version 4.0, Wiley Interdisciplinary Reviews: Computational Molecular Science 8(1) (2018) e1327.
[31] T. Lu, Q. Chen, Independent gradient model based on Hirshfeld partition: A new method for visual study of interactions in chemical systems, J. Comput. Chem. 43 (8) (2022) 539–555.
[32] T. Lu, F. Chen, Multiwfn: A multifunctional wavefunction analyzer, J. Comput. Chem. 33 (5) (2012) 580–592.
[33] W. Humphrey, A. Dalke, K. Schulten, VMD: visual molecular dynamics, J. Mol. Graph. 14 (1) (1996) 33–38.
[34] L. Zhao, S. Sun, J. Lin, L. Zhong, L. Chen, J. Guo, J. Yin, H.N. Alshareef, X. Qiu, W. Zhang, Defect engineering of disordered carbon anodes with ultra-high heteroatom doping through a supermolecule-mediated strategy for potassium-ion hybrid capacitors, Nano-Micro Lett. 15 (1) (2023) 41.
[35] X. Yue, T. Suopajärvi, S. Sun, O. Mankinen, A. Mikkelson, H. Huttunen, S. Komulainen, I. Romakkaniemi, J. Ahola, V.-V. Telkki, High-purity lignin fractions and nanospheres rich in phenolic hydroxyl and carboxyl groups isolated with alkaline deep eutectic solvent from wheat straw, Bioresour. Technol. 360 (2022), 127570.
[36] K.A. Jung, S.H. Woo, S.-R. Lim, J.M. Park, Pyrolytic production of phenolic compounds from the lignin residues of bioethanol processes, Chem. Eng. J. 259 (2015) 107–116.
[37] S.J. Lee, H.J. Kim, E.J. Cho, Y. Song, H.-J. Bae, Isolation and characterization of lignin from the oak wood bioethanol production residue for adhesives, Int. J. Biol. Macromol. 72 (2015) 1056–1062.
[38] P.G. Gan, S.T. Sam, M.F. Abdullah, M.F. Omar, L.S. Tan, An alkaline deep eutectic solvent based on potassium carbonate and glycerol as pretreatment for the isolation of cellulose nanocrystals from empty fruit bunch, BioResources 15 (1) (2020) 1154–1170.
[39] X. Tang, M. Zuo, Z. Li, H. Liu, C. Xiong, X. Zeng, Y. Sun, L. Hu, S. Liu, T. Lei, Green processing of lignocellulosic biomass and its derivatives in deep eutectic solvents, ChemSusChem 10 (13) (2017) 2696–2706.
[40] L. Fan, Y. Zhang, S. Liu, N. Zhou, P. Chen, Y. Cheng, M. Addy, Q. Lu, M.M. Omar, Y. Liu, Bio-oil from fast pyrolysis of lignin: Effects of process and upgrading parameters, Bioresour. Technol. 241 (2017) 1118–1126.
[41] T. Yokoyama, Revisiting the mechanism of β–O–4 bond cleavage during acidolysis of lignin. Part 6: A review, J. Wood Chem. Technol. 35 (1) (2015) 27–42.
[42] S. Hong, X.-J. Shen, B. Pang, Z. Xue, X.-F. Cao, J.-L. Wen, Z.-H. Sun, S.S. Lam, T.-Q. Yuan, R.-C. Sun, In-depth interpretation of the structural changes of lignin and

formation of diketones during acidic deep eutectic solvent pretreatment, Green Chem. 22 (6) (2020) 1851–1858.
[43] C. Liu, J. Hu, H. Zhang, R. Xiao, Thermal conversion of lignin to phenols: Relevance between chemical structure and pyrolysis behaviors, Fuel 182 (2016) 864–870.
[44] A. Tolbert, H. Akinosho, R. Khunsupat, A.K. Naskar, A.J. Ragauskas, Characterization and analysis of the molecular weight of lignin for biorefining studies, Biofuels Bioprod. Biorefin. 8 (6) (2014) 836–856.
[45] X.-J. Shen, T. Chen, H.-M. Wang, Q. Mei, F. Yue, S. Sun, J.-L. Wen, T.-Q. Yuan, R.-C. Sun, Structural and morphological transformations of lignin macromolecules during bio-based deep eutectic solvent (DES) pretreatment, ACS Sustain. Chem. Eng. 8 (5) (2019) 2130–2137.
[46] P. Merdy, E. Guillon, J. Dumonceau, M. Aplincourt, Characterisation of a wheat straw cell wall residue by various techniques: A comparative study with a synthetic and an extracted lignin, Anal. Chim. Acta 459 (1) (2002) 133–142.
[47] D. Kocaefe, X. Huang, Y. Kocaefe, Y. Boluk, Quantitative characterization of chemical degradation of heat-treated wood surfaces during artificial weathering using XPS, Surf. Interface Anal. 45 (2) (2013) 639–649.
[48] Z. Ma, S. Li, G. Fang, N. Patil, N. Yan, Modification of chemical reactivity of enzymatic hydrolysis lignin by ultrasound treatment in dilute alkaline solutions, Int. J. Biol. Macromol. 93 (2016) 1279–1284.
[49] P. De Lange, A. De Kreek, A. Van Linden, N. Coenjaarts, Weathering of wood and protection by chromium studied by XPS, Surf. Interface Anal. 19 (1–12) (1992) 397–402.
[50] M. Balakshin, E. Capanema, On the quantification of lignin hydroxyl groups with 31P and 13C NMR spectroscopy, J. Wood Chem. Technol. 35 (3) (2015) 220–237.
[51] T. Li, Y. Yin, S. Wu, X. Du, Effect of deep eutectic solvents-regulated lignin structure on subsequent pyrolysis products selectivity, Bioresour. Technol. 343 (2022), 126120.
[52] X. Du, M. Pérez-Boada, C. Fernández, J. Rencoret, J.C. Del Río, J. Jiménez-Barbero, J. Li, A. Gutiérrez, A.T. Martínez, Analysis of lignin–carbohydrate and lignin–lignin linkages after hydrolase treatment of xylan–lignin, glucomannan–lignin and glucan–lignin complexes from spruce wood, Planta 239 (2014) 1079–1090.
[53] R. Jastrzebski, S. Constant, C.S. Lancefield, N.J. Westwood, B.M. Weckhuysen, P. C. Bruijnincx, Tandem catalytic depolymerization of lignin by water-tolerant Lewis acids and rhodium complexes, ChemSusChem 9 (16) (2016) 2074–2079.
[54] C. Zhao, J. Huang, L. Yang, F. Yue, F. Lu, Revealing structural differences between alkaline and kraft lignins by HSQC NMR, Ind. Eng. Chem. Res. 58 (14) (2019) 5707–5714.
[55] R. Samuel, Y. Pu, B. Raman, A.J. Ragauskas, Structural characterization and comparison of switchgrass ball-milled lignin before and after dilute acid pretreatment, Appl. Biochem. Biotechnol. 162 (2010) 62–74.
[56] M. Alekhina, O. Ershova, A. Ebert, S. Heikkinen, H. Sixta, Softwood kraft lignin for value-added applications: Fractionation and structural characterization, Ind. Crops Prod. 66 (2015) 220–228.
[57] B.B. Hallac, Y. Pu, A.J. Ragauskas, Chemical transformations of Buddleja davidii lignin during ethanol organosolv pretreatment, Energy Fuels 24 (4) (2010) 2723–2732.
[58] T. Faravelli, A. Frassoldati, G. Migliavacca, E. Ranzi, Detailed kinetic modeling of the thermal degradation of lignins, Biomass Bioenerg. 34 (3) (2010) 290–301.
[59] Z. Chen, X. Bai, H. Zhang, C. Wan, Insights into structural changes of lignin toward tailored properties during deep eutectic solvent pretreatment, ACS Sustain. Chem. Eng. 8 (26) (2020) 9783–9793.
[60] Z. Guo, J. Mao, Q. Zhang, F. Xu, Integrated biorefinery of bamboo for fermentable sugars, native-like lignin, and furfural production by novel deep eutectic solvents treatment, Ind. Crops Prod. 188 (2022), 115453.
[61] G. Lyu, Q. Wu, T. Li, W. Jiang, X. Ji, G. Yang, Thermochemical properties of lignin extracted from willow by deep eutectic solvents (DES), Cellul. 26 (2019) 8501–8511.
[62] H. Kawamoto, M. Ryoritani, S. Saka, Different pyrolytic cleavage mechanisms of β–ether bond depending on the side-chain structure of lignin dimers, J. Anal. Appl. Pyrolysis 81 (1) (2008) 88–94.
[63] S. Wang, B. Ru, H. Lin, W. Sun, Z. Luo, Pyrolysis behaviors of four lignin polymers isolated from the same pine wood, Bioresour. Technol. 182 (2015) 120–127.
[64] A.G. Margellou, C.P. Pappa, E.A. Psochia, M.D. Petala, K.S. Triantafyllidis, Mild isolation and characterization of surface lignin from hydrothermally pretreated lignocellulosic forestry and agro-industrial waste biomass, Sustain. Chem. Pharm. 33 (2023), 101056.
[65] Y. Zhang, Y. Gao, M. Zhao, X. Feng, L. Wang, H. Yang, H. Ma, J. Zhou, Effects of torrefaction on the lignin of apricot shells and Its catalytic conversion to aromatics, ACS Omega 6 (39) (2021) 25742–25748.
[66] Y. Fan, Z. Zhang, Z. Wang, H. Yu, X. Kong, P. Li, M. Li, R. Xiao, C. Liu, Radical footprinting and regularity revealing during the pyrolysis of technical lignins, Bioresour. Technol. 360 (2022), 127648.
[67] M. Lei, S. Wu, J. Liang, C. Liu, Comprehensive understanding the chemical structure evolution and crucial intermediate radical in situ observation in enzymatic hydrolysis/mild acidolysis lignin pyrolysis, J. Anal. Appl. Pyrolysis 138 (2019) 249–260.
[68] A. Trubetskaya, P.A. Jensen, A.D. Jensen, P. Glarborg, F.H. Larsen, M.L. Andersen, Characterization of free radicals by electron spin resonance spectroscopy in biochars from pyrolysis at high heating rates and at high temperatures, Biomass Bioenerg. 94 (2016) 117–129.
[69] Q. Zheng, Z. Li, T. Guo, Q. Fan, S. Hu, J. Xiang, P. Fu, Unraveling the synergistic development of carbon skeleton and pore networks involved in lignin pyrolysis, J. Anal. Appl. Pyrolysis 170 (2023), 105912.